

Interplay of thermalization and strong disorder: Wave turbulence theory, numerical simulations, and experiments in multimode optical fibers

Nicolas Berti¹, Kilian Baudin¹, Adrien Fusaro², Guy Millot^{1,3}, Antonio Picozzi¹, Josselin Garnier⁴

¹ *Laboratoire Interdisciplinaire Carnot de Bourgogne, CNRS, Université Bourgogne Franche-Comté, Dijon, France*

² *CEA, DAM, DIF, F-91297 Arpajon Cedex, France*

³ *Institut Universitaire de France (IUF), 1 rue Descartes, 75005 Paris, France and*

⁴ *CMAF, CNRS, Ecole Polytechnique, Institut Polytechnique de Paris, 91128 Palaiseau Cedex, France*

We address the problem of thermalization in the presence of a time-dependent disorder in the framework of the nonlinear Schrödinger (or Gross-Pitaevskii) equation with a random potential. The thermalization to the Rayleigh-Jeans distribution is driven by the nonlinearity. On the other hand, the structural disorder is responsible for a relaxation toward the homogeneous equilibrium distribution (particle equipartition), which thus inhibits thermalization (energy equipartition). On the basis of the wave turbulence theory, we derive a kinetic equation that accounts for the presence of strong disorder. The theory unveils the interplay of disorder and nonlinearity. It unexpectedly reveals that a non-equilibrium process of condensation and thermalization can take place in the regime where disorder effects dominate over nonlinear effects. We validate the theory by numerical simulations of the nonlinear Schrödinger equation and the derived kinetic equation, which are found in quantitative agreement without using adjustable parameters. Experiments realized in multimode optical fibers with an applied external stress evidence the process of thermalization in the presence of strong disorder.

Introduction.— A non-integrable Hamiltonian system of random waves is expected to exhibit a process of thermalization, which is characterized by an irreversible evolution toward the thermodynamic equilibrium state of maximum entropy. In the weakly nonlinear regime, this process is described in detail by the well-developed wave turbulence theory [1–9]. In spite of the formal reversibility of the Hamiltonian system, the wave turbulence kinetic equation describes the actual irreversible evolution to the Rayleigh-Jeans (RJ) equilibrium distribution. RJ thermalization can be characterized by a process of wave condensation that is featured by the macroscopic population of the fundamental mode of the system [2–4, 10–18]. This phenomenon received a recent renewed interest with the discovery of spatial beam cleaning in multimode optical fibers (MMFs) [19–21]. Along this line, RJ thermalization and light condensation in MMFs have been discussed [22–28] and recently observed experimentally [29–33].

On the other hand, a structural disorder of the nonlinear medium is known to deeply affect the coherence properties of the waves. Understanding the interplay of nonlinearity and disorder is a fundamental problem, in relation with the paradigm of statistical light-mode dynamics, glassy behaviors and complexity science [34–42]. Disorder is also known to impact light propagation in MMFs, a feature relevant to endoscopic imaging [43, 44], or to study completely integrable Manakov systems [45–48]. Due to refractive index fluctuations introduced by inherent imperfections and environmental perturbations, a MMF leads to both polarization mixing and random mode coupling [45–49]. While polarization random fluctuations, i.e., *weak disorder*, have been shown to acceler-

ate the process of beam-cleaning condensation in MMFs [23, 25], so far, the interplay of *strong disorder* (i.e., random coupling among non-degenerate modes) and thermalization has not yet been considered.

In this Letter we address the problem of thermalization of random waves that propagate in a disordered system by considering the representative example of the Nonlinear Schrödinger (NLS), or Gross-Pitaevskii, equation with a time-dependent random potential. On the basis of the wave turbulence theory [1–9], we derive a kinetic equation (KE) that accounts for the presence of a time-dependent strong disorder. Our theory describes in detail the *antagonist impacts of nonlinearity and disorder*: While strong disorder enforces a relaxation to the homogeneous equilibrium distribution of the modal components (‘particle’ equipartition, $w_j^{\text{eq}} = \text{const}$, w_j being the occupation of the j -th mode), the nonlinear process of thermalization favours the macroscopic population of the condensed fundamental mode ($w_0 \gg w_j$ for $j \neq 0$). The remarkable result of our work is to show that, despite the dominant strength of disorder, the system can exhibit an unexpected process of *non-equilibrium condensation* in the initial evolution stage, while the system eventually relaxes to the homogeneous equilibrium distribution dictated by strong disorder. The theory is confirmed by intensive numerical simulations of the NLS equation, which are found in quantitative agreement with the simulations of the derived KE, *without using any adjustable parameter*. We report experiments in MMFs with an applied external stress to control the strength of disorder, which evidences the process of RJ thermalization and condensation in the presence of strong disorder.

Our work paves the way for the development of a systematic method to tackle the impact of a *time-dependent disorder in wave turbulence* – our methodology substantially differs from that developed for a time-independent disorder [38–42]. More generally this work contributes to the understanding of spontaneous organization of coherent states in nonlinear disordered systems [34–38].

NLS equation with random potential.– We consider the general form of the stochastic NLS equation

$$i\partial_z\psi = -\alpha\nabla^2\psi + V(\mathbf{r})\psi - \gamma|\psi|^2\psi + \delta V(\mathbf{r}, z)\psi. \quad (1)$$

It governs the transverse spatial evolution of an optical beam propagating along the z -axis of a waveguide, whose ideal transverse index profile is $V(\mathbf{r})$ [$\mathbf{r} = (x, y)$], while $\delta V(z, \mathbf{r})$ is the ‘time’-dependent random perturbation of the potential ($\langle\delta V\rangle = 0$). The parameters α and γ denote the linear and nonlinear coefficients. The disorder being (‘time’) z -dependent, our system is of different nature than those studying the interplay of thermalization and Anderson localization [38–42].

We expand the field $\psi(z, \mathbf{r}) = \sum_j a_j(z)u_j(\mathbf{r})$ on the basis of the M real-valued eigenmodes $u_j(\mathbf{r})$ (solution of $\beta_j u_j = -\alpha\nabla^2 u_j + V(\mathbf{r})u_j$) of the unperturbed waveguide. The mode amplitudes $a_j(z)$ satisfy

$$i\partial_z a_j = \beta_j a_j - \gamma \sum_{l,m,n} Q_{jlmn} a_l a_m a_n^* + \sum_l C_{jl}(z) a_l, \quad (2)$$

where $Q_{jlmn} = \int u_j(\mathbf{r})u_l(\mathbf{r})u_m(\mathbf{r})u_n(\mathbf{r})d\mathbf{r}$ denotes the mode overlap, and the random mode coupling matrix reads

$$C_{jl}(z) = \int u_j(\mathbf{r})\delta V(z, \mathbf{r})u_l(\mathbf{r})d\mathbf{r}. \quad (3)$$

The stochastic NLS Eq.(1) and the modal NLS Eq.(2) are equivalent. They conserve the total power (particle number) $N = \int |\psi|^2 d\mathbf{r} = \sum_j |a_j|^2$, while the random potential $\delta V(\mathbf{r}, z)$ in Eq.(1) (or $\mathbf{C}(z)$ in Eq.(2)), prevents the conservation of the energy (Hamiltonian).

Kinetic equation.– We consider the situation where the random potential is a weak perturbation with respect to linear propagation effects ($\delta V \ll V$), i.e. $L_{lin} = 1/\beta_0 \ll L_{dis} = 1/\sigma$ and $L_{lin} \ll \ell_c$, where σ^2 denotes the variance of the fluctuations of the random potential (i.e., ‘strength’ of disorder) and ℓ_c the corresponding correlation length. Note that this is the usual case in an optical waveguide configuration, e.g., in MMFs. Furthermore, we assume that disorder dominates over nonlinear effects $L_{dis} \ll L_{nl} \simeq 1/(\gamma \langle |\psi|^2 \rangle)$.

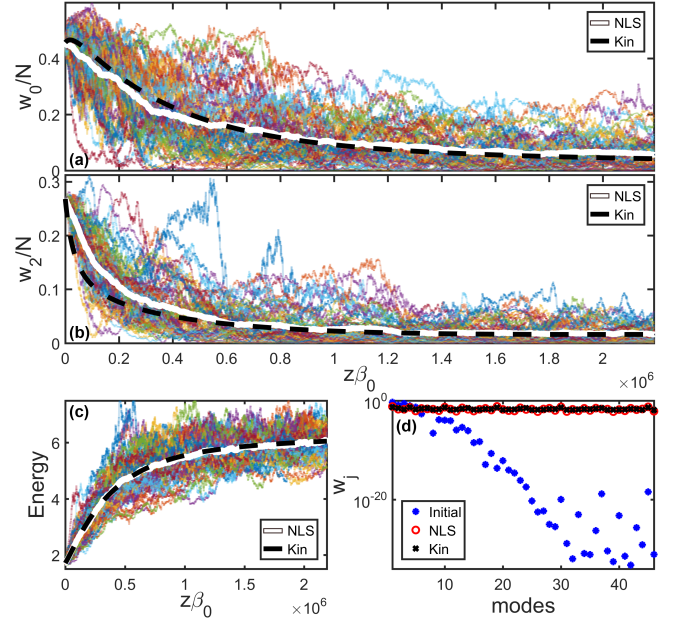


FIG. 1: **Dynamics dominated by strong disorder** $\mathcal{L}_{kin}^{RJ} \gg \mathcal{L}_{kin}^{eq}$: The system irreversibly relaxes toward the equilibrium w_j^{eq} . Evolutions of the fundamental mode $w_0(z)$ (a), and $w_2(z)$ (b), the energy $E(z)/(N\beta_0)$ (c), obtained from the numerical simulation of the NLS Eq.(2): 64 realizations are reported with colored lines; the bold white line is the corresponding empirical average; the dashed black line is the prediction of the KE (4). (d) Modal distribution w_j in the initial condition ($z = 0$, blue) and at $z\beta_0 = 2 \times 10^6$ for the NLS simulation (red), and the KE (black). Parameters: $L_{dis}/L_{lin} = 7$, $L_{dis}/L_{nl} = 4.1 \times 10^{-4}$, $\ell_c\beta_0 = 42$.

We develop a wave turbulence theory [1–9] accounting for a time-dependent disorder by exploiting tools inherited from the asymptotic analysis of randomly driven ordinary differential equations [50]. We derive the KE governing the evolution of the averaged modal components $w_j(z) = \langle |a_j(z)|^2 \rangle$ [51]:

$$\partial_z w_j = \sum_{l \neq j} \Gamma_{jl}^{OD} (w_l - w_j) + Coll[\mathbf{w}] \quad (4)$$

where the collision term reads

$$Coll[\mathbf{w}] = 8\gamma^2 \sum_{l,m,n} \frac{\delta_{jlmn}^K Q_{jlmn}^2}{G_{jlmn}^D} R_{jlmn}[\mathbf{w}],$$

$$R_{jlmn}[\mathbf{w}] = w_l w_m w_j + w_l w_m w_n - w_j w_n w_m - w_j w_n w_l,$$

and the Kronecker symbol denotes a frequency resonance ($\delta_{jlmn}^K = 1$ if $\Delta\beta_{jlmn} = \beta_j - \beta_l - \beta_m + \beta_n = 0$, and zero otherwise). For clarity, we assume that the modes are not degenerate – see [51] for the KE accounting for mode degeneracies.

The KE (4) unveils the interplay of nonlinearity and disorder. It reveals that diagonal and off-diagonal elements of the random matrix \mathbf{C} play fundamental different roles. The first term in the KE (4) originates in

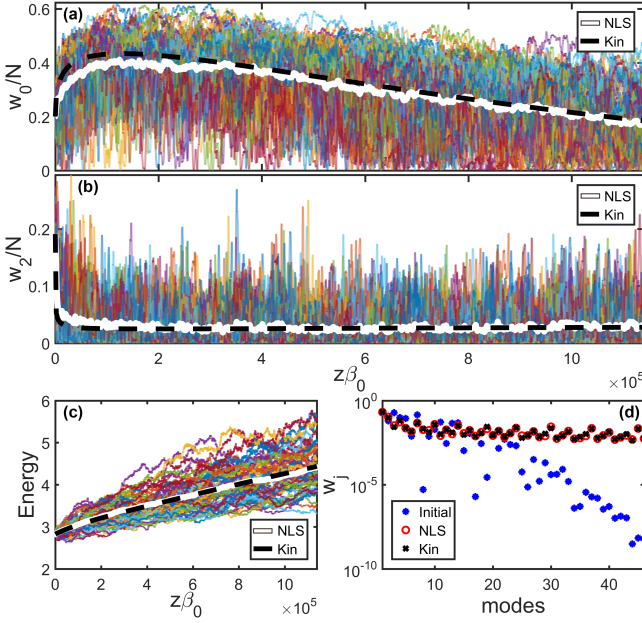


FIG. 2: **Thermalization precedes equilibrium relaxation:** Same panels as in Fig. 1, but in the regime $\mathcal{L}_{\text{kin}}^{\text{RJ}} \lesssim \mathcal{L}_{\text{kin}}^{\text{eq}}$. The system exhibits an incipient process of RJ thermalization and nonequilibrium condensation characterized by a growth of the condensate amplitude $w_0(z)$ for $z\beta_0 \lesssim 2 \times 10^5$. Disorder subsequently prevails, which induces a decay of $w_0(z)$ (and eventually brings the system to equilibrium w_j^{eq}). Parameters: $L_{\text{dis}}/L_{\text{lin}} = 7$, $L_{\text{dis}}/L_{\text{nl}} = 0.033$, $\ell_c\beta_0 = 167$.

off-diagonal elements of C_{jl} ($j \neq l$):

$$\Gamma_{jl}^{\text{OD}} = 2 \int_0^\infty \langle C_{jl}(0)C_{jl}(z) \rangle \cos((\beta_j - \beta_l)z) dz. \quad (5)$$

It describes an irreversible relaxation toward the homogeneous distribution featured by an equipartition of ‘particles’ among the modes, $w_j^{\text{eq}} = N/M = \text{const}$. This process occurs over the typical propagation length [52]

$$\mathcal{L}_{\text{kin}}^{\text{eq}} \simeq 1/\overline{\Gamma_{jl}^{\text{OD}}}. \quad (6)$$

This is the well-known evolution of a system ruled by random mode coupling.

We now show that this relaxation process mediated by strong disorder *does not necessarily inhibit the nonlinear processes of thermalization and condensation*. This becomes apparent through the collision term in the KE (4), which exclusively involves the *diagonal* components C_{jj} :

$$\Gamma_{jl}^{\text{D}} = \int_0^\infty \langle C_{jj}(0)C_{ll}(z) \rangle + \langle C_{ll}(0)C_{jj}(z) \rangle dz. \quad (7)$$

The matrix Γ^{D} contributes to the tensor involved in the collision term, $G_{jlmn}^{\text{D}} = \Gamma_{ll}^{\text{D}} + \Gamma_{mm}^{\text{D}} + \Gamma_{nn}^{\text{D}} + \Gamma_{jj}^{\text{D}} + 2\Gamma_{lm}^{\text{D}} - 2\Gamma_{ln}^{\text{D}} - 2\Gamma_{lj}^{\text{D}} - 2\Gamma_{mn}^{\text{D}} - 2\Gamma_{mj}^{\text{D}} + 2\Gamma_{nj}^{\text{D}}$ [51]. To discuss the role of the collision term, we forget for a while the first

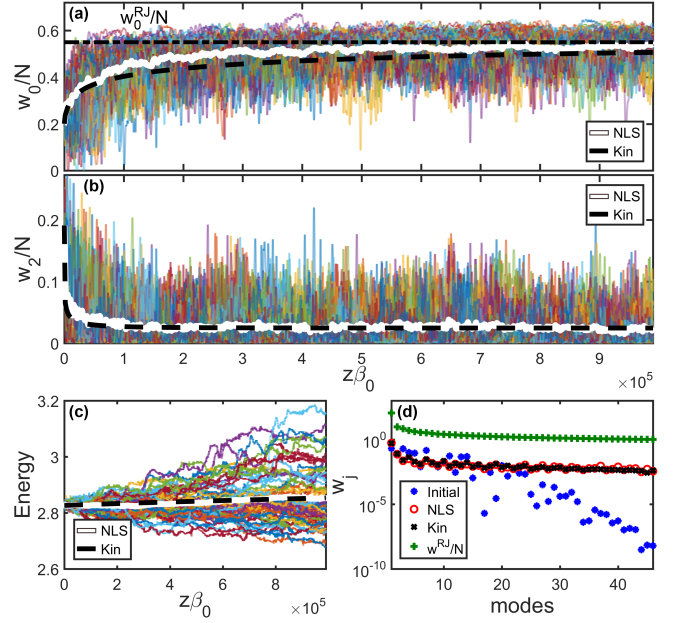


FIG. 3: **Thermalization prevails over equilibrium relaxation:** Same panels as in Fig. 1, but in the regime $\mathcal{L}_{\text{kin}}^{\text{RJ}} \ll \mathcal{L}_{\text{kin}}^{\text{eq}}$. The system exhibits a process of RJ thermalization and condensation characterized by a significant growth of the condensate amplitude $w_0(z)$ to the value predicted by the RJ distribution, $w_0^{\text{RJ}}/N \simeq 0.55$ (horizontal dashed-dotted black line) (a). At variance with Figs. 1-2, the energy $E(z)$ is almost constant (c). The modes approach the RJ distribution w_j^{RJ} (green) (d). Parameters: $L_{\text{dis}}/L_{\text{lin}} = 8.4$, $L_{\text{dis}}/L_{\text{nl}} = 0.04$, $\ell_c\beta_0 = 4 \times 10^3$.

term in the KE (4). The collision term conserves $N = \sum_j w_j(z)$, $E = \sum_j \beta_j w_j(z)$, and exhibits a H -theorem of entropy growth $\partial_z S \geq 0$, with $S(z) = \sum_j \log[w_j(z)]$ [51]. Hence, it describes a process of thermalization to the RJ distribution $w_j^{\text{RJ}} = T/(\beta_j - \mu)$, which occurs over a typical propagation length

$$\mathcal{L}_{\text{kin}}^{\text{RJ}} \simeq L_{\text{nl}}^2 \overline{G_{jlmn}^{\text{D}}}/Q_{jlmn}^2. \quad (8)$$

For an energy smaller than a critical value $E \leq E_{\text{crit}} \simeq N\beta_0\sqrt{M/2}$, the RJ distribution w_j^{RJ} exhibits a phase transition to a condensed state [29]. The condensate amplitude w_0 then constitutes the natural parameter that distinguishes the two antagonist regimes:

- (i) For $\mathcal{L}_{\text{kin}}^{\text{eq}} \ll \mathcal{L}_{\text{kin}}^{\text{RJ}}$, the disorder dominates and $w_0(z) \rightarrow w_j^{\text{eq}} = N/M = \text{const}$ for $j = 0, 1, \dots, M-1$;
- (ii) For $\mathcal{L}_{\text{kin}}^{\text{eq}} \gg \mathcal{L}_{\text{kin}}^{\text{RJ}}$, the dynamics is dominated by RJ thermalization, and condensation leads to a macroscopic population of the fundamental mode $w_0(z) \rightarrow w_0^{\text{RJ}} \gg w_j^{\text{RJ}}$ for $j = 1, \dots, M-1$.

Numerical simulations.— We have performed numerical simulations to test the validity of our theory. We have considered the concrete example of a parabolic trapping potential of the form $V(\mathbf{r}) = q_x x^2 + q_y y^2$, with the fundamental mode eigenvalue $\beta_0 = \sqrt{\alpha}(\sqrt{q_x} + \sqrt{q_y})$. We consider a general model of disorder with a random potential of the form $\delta V(\mathbf{r}, z) = \mu(z)g(\mathbf{r})$, where $\mu(z)$ is a real-valued stochastic function with zero mean and $\langle \mu(0)\mu(z) \rangle = \sigma^2 \exp(-|z|/\ell_c)$. In order to remove mode degeneracies, we consider in the simulations an elliptical parabolic potential ($q_x \neq q_y$). To compute the matrices Γ^{OD} and Γ^{D} in analytical form we consider $g(x, y) = \cos(b_x x/x_0) \cos(b_y y/y_0)$, where (x_0, y_0) denote the radii of the fundamental elliptical mode [51].

According to the theory, the two terms in the KE (4) are antagonists and compete against each other. If $\mathcal{L}_{\text{kin}}^{\text{eq}} \ll \mathcal{L}_{\text{kin}}^{\text{RJ}}$, disorder prevails and the system relaxes to the expected equilibrium $w_j^{\text{eq}} = \text{const}$. This is illustrated in Fig. 1, which reports the results of the numerical integration of the NLS Eq.(2) for 64 realizations ($\mathcal{L}_{\text{kin}}^{\text{RJ}}/\mathcal{L}_{\text{kin}}^{\text{eq}} \simeq 400$). The corresponding average over such realizations (bold white line) is in agreement with the simulation of the KE (4) (dashed black line) starting from the same initial condition. Here and thereafter, the quantitative agreement between NLS and KE simulations is obtained without any adjustable parameter.

Unexpectedly, however, a *nonequilibrium* process of condensation and thermalization can be observed in the initial stage of propagation when $\mathcal{L}_{\text{kin}}^{\text{RJ}} \lesssim \mathcal{L}_{\text{kin}}^{\text{eq}}$ (see Fig. 2 for $\mathcal{L}_{\text{kin}}^{\text{RJ}}/\mathcal{L}_{\text{kin}}^{\text{eq}} \simeq 0.07$), while asymptotically the system still relaxes to the homogeneous equilibrium state w_j^{eq} . The nonequilibrium property of condensation is reflected by the fact that the energy $E(z) = \sum_j \beta_j w_j(z)$ is *not conserved during the evolution*, see Fig. 2(c).

We stress that the condensation processes can occur very efficiently by increasing the correlation length ℓ_c , in such a way that $\mathcal{L}_{\text{kin}}^{\text{RJ}} \ll \mathcal{L}_{\text{kin}}^{\text{eq}}$, see Fig. 3 for $\mathcal{L}_{\text{kin}}^{\text{RJ}}/\mathcal{L}_{\text{kin}}^{\text{eq}} \simeq 0.003$. In this regime, the energy is almost conserved $E \simeq \text{const}$ and RJ thermalization occurs almost completely, as confirmed by the modal populations that approach the RJ distribution w_j^{RJ} (Fig. 3(d)), and the condensate approaches the RJ prediction $w_0^{\text{RJ}}/N \simeq 0.55$, see Fig. 3(a). Note that, for $z \gg \mathcal{L}_{\text{kin}}^{\text{eq}}$, the system would still relax to the equilibrium w_j^{eq} .

Experiments.— We performed experiments in a MMF to evidence light condensation in the presence of strong disorder. The subnanosecond pulses delivered by a Nd:YAG laser ($\lambda = 1.06\mu\text{m}$) are passed through a diffuser before injection into a 12m long graded-index MMF (i.e., parabolic-shaped potential $V(\mathbf{r})$) that guides $M \simeq 120$ modes. We measure the power N and the energy E from the near-field and far-field measurements of the intensity distributions at the fiber output, see Ref.[29] for details.

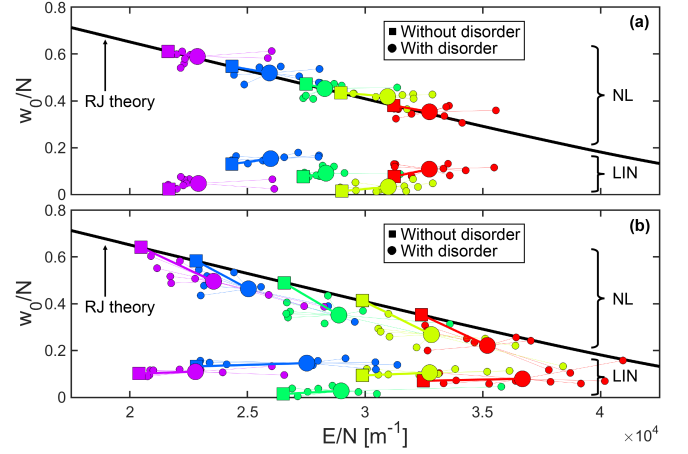


FIG. 4: Observation of light condensation with strong disorder: Measurements of the condensate fraction w_0/N vs E/N at small power [linear (LIN) regime] and high power [nonlinear (NL) regime], for a moderate (a), and a large (b), strength of random mode coupling. The solid line reports the prediction from the RJ theory, w_0^{RJ}/N . In the absence of strong disorder (squares): w_0/N increases as the power increases, and reaches the RJ prediction (solid line) – each color refers to a different value of E/N . In the presence of strong disorder (big circles): the energy E/N increases due to disorder (squares are shifted to big circles of the same color), by $\Delta E/N \simeq 6\%$ (a), and $\Delta E/N \simeq 11\%$ (b). The big circles report the average over 10 different realizations of disorder (10 small circles for each color). RJ thermalization takes place in the presence of strong disorder (a), and it is quenched by further increasing the amount of disorder (b) [51].

Here, the originality with respect to *all previous experiments* on beam cleaning condensation and thermalization [19–21, 29–32], is that we introduce strong disorder in the experiment. Strong mode coupling is obtained by applying a stress to the MMF with clamps [49]. By adjusting the applied stress, we can tune the strength of mode coupling (i.e., σ). In the absence of an applied stress, polarization coupling and random coupling among degenerate modes take place: In this *weak random coupling regime* the energy $E = \sum_j \beta_j w_j$ is conserved during light propagation in the MMF [23, 25], as confirmed by direct experimental measurements [24, 29–32]. Here, we apply stress on the MMF to induce a random coupling among *non-degenerate modes* [45–48, 53]. In this regime of *strong mode coupling*, the energy E is no longer conserved through propagation in the MMF. Note that, it would be difficult, or even impossible, to accurately model in the simulations the peculiar form of disorder induced by the applied stress on the fiber. Furthermore, the simulations reported above do not account for the mode degeneracies of the fiber used in the experiments. Accordingly, the simulations do not describe quantitatively our experiments.

We report in Fig. 4(a) the measurements of the condensate fraction w_0/N at small power (linear regime),

strong power (nonlinear regime), and in the presence, or absence, of applied stress. Following Ref.[29], the diffruser allows us to vary the energy density E/N of the injected speckle beam: The squares in Fig. 4(a) report the corresponding condensate fractions w_0/N in the linear and nonlinear regimes in the *absence of strong disorder*. For each speckle beam with energy E/N (i.e., for each color in Fig. 4(a)), we apply stress on different points of the fiber to get an ensemble of 10 realizations with disorder. We report in Fig. 4(a) the corresponding values of w_0/N for such 10 realizations (small circles), as well as the corresponding average over realizations (large circles). Because the applied stress on the MMF induces power losses (10% in Fig. 4(a)) [49], we normalize the energy with respect to the (average) power: $E/N = \sum_j \beta_j w_j / \sum_j w_j = \bar{\beta}_j$. Strong random mode coupling leads to an *increase* of E/N , as evidenced in Fig. 4(a) where the squares are shifted to the big circles by an amount of $\Delta E/N \simeq 6\%$: The larger the strength of applied stress, the larger the energy shift $\Delta E/N$.

Figure 4(a) remarkably reveals that, by increasing the power from the linear regime ($N = 0.23\text{kW}$) to the nonlinear regime ($N = 7\text{kW}$), the condensate fraction w_0/N (big circles) increases and approaches the value predicted by the RJ distribution w_0^{RJ}/N (solid line). Thermalization then takes place: (i) in the presence of strong disorder, i.e., in the presence of an energy shift $\Delta E/N$; (ii) over a broad range of E/N , i.e., broad range of condensate fractions. Note that, the presence of losses, distributed either homogeneously or non-homogeneously among the modes, does not significantly affect the condensate fraction [51].

We have repeated the procedure of Fig. 4(a) by increasing the applied stress on the MMF with an energy shift $\Delta E/N \simeq 11\%$ (20% of power losses). As evidenced in Fig. 4(b), $\Delta E/N$ is larger than in Fig. 4(a). Consequently, the condensate fractions w_0/N in the nonlinear regime no longer reach the RJ prediction, i.e., strong disorder prevents a complete process of RJ thermalization and condensation. By further increasing the applied stress and the corresponding energy shift $\Delta E/N \simeq 19\%$, our experimental results show that *RJ thermalization is inhibited by strong disorder*, see [51].

Conclusion.- We have developed a wave turbulence theory that accounts for a ‘time’-dependent disorder by considering the NLS equation with a random potential. Simulations of the derived KE (4) are found in quantitative agreement with NLS simulations, *without using any adjustable parameter*. The theory remarkably reveals that RJ thermalization and condensation can take place efficiently in the presence of strong disorder, as confirmed by experiments realized in MMFs.

The developed wave turbulence theory can be extended to dissipative systems [54, 55], or to different types of disordered nonlinear systems, e.g., Bose-Einstein condensates, hydrodynamics, condensed matter, etc.

Acknowledgments.- The authors are grateful to K. Krupa and S. Rica for fruitful discussions. Fundings: Centre national de la recherche scientifique (CNRS), Conseil régional de Bourgogne Franche-Comté, iXCore Research Fondation, Agence Nationale de la Recherche (ANR-19-CE46-0007, ANR-15-IDEX-0003, ANR-21-ESRE-0040). Calculations were performed using HPC resources from DNUM CCUB (Centre de Calcul, Université de Bourgogne).

SUPPLEMENTARY MATERIAL

DERIVATION OF THE KINETIC EQ.(4)

Primary asymptotics

The starting point is the NLS Eq.(1) written in the mode basis, i.e., Eq.(2). We consider the regime where linear propagation dominates over disorder, which in turn dominates over the nonlinearity. Accordingly, we introduce a small dimensionless parameter ε and we consider the regime $\beta_j \rightarrow \beta_j, \mathbf{C} \rightarrow \varepsilon \mathbf{C}, \gamma \rightarrow \varepsilon^2 \gamma$. For propagation distances of order ε^{-2} , the rescaled mode amplitudes $a_j^\varepsilon(z) = a_j(z/\varepsilon^2)$ satisfy

$$\partial_z a_j^\varepsilon = -i \frac{\beta_j}{\varepsilon^2} a_j^\varepsilon + i\gamma \sum_{l,m,n=0}^{M-1} Q_{jlmn} a_l^\varepsilon a_m^\varepsilon \bar{a}_n^\varepsilon - \frac{i}{\varepsilon} \sum_{l=0}^{M-1} C_{jl} \left(\frac{z}{\varepsilon^2}\right) a_l^\varepsilon,$$

where the bar stands for complex conjugation. We set $c_j^\varepsilon(z) = a_j^\varepsilon(z) \exp(i \frac{\beta_j}{\varepsilon^2} z)$. The amplitudes $c_j^\varepsilon(z)$ satisfy:

$$\begin{aligned} \partial_z c_j^\varepsilon &= i\gamma \sum_{l,m,n=0}^{M-1} Q_{jlmn} c_l^\varepsilon c_m^\varepsilon \bar{c}_n^\varepsilon \exp(i \frac{\beta_j - \beta_l - \beta_m + \beta_n}{\varepsilon^2} z) \\ &\quad - \frac{i}{\varepsilon} \sum_{l=0}^{M-1} C_{jl} \left(\frac{z}{\varepsilon^2}\right) c_l^\varepsilon \exp(i \frac{\beta_j - \beta_l}{\varepsilon^2} z). \end{aligned} \quad (9)$$

This is the usual diffusion approximation framework [50]. We get the following result.

Proposition .1 *The random process $(c_j^\varepsilon(z))_{j=0}^{M-1}$ converges in distribution in $\mathcal{C}^0([0, \infty), \mathbb{C}^M)$, the space of continuous functions from $[0, \infty)$ to \mathbb{C}^M , to the Markov process $(\mathbf{c}_j(z))_{j=0}^{M-1}$ with infinitesimal generator \mathcal{L} :*

$$\mathcal{L} = \mathcal{L}_1 + \mathcal{L}_2 + \mathcal{L}_3 + \mathcal{L}_4 + \mathcal{L}_5, \quad (10)$$

with

$$\begin{aligned} \mathcal{L}_1 &= \frac{1}{2} \sum_{j,l=0, j \neq l}^{M-1} \Gamma_{jl}^{\text{OD}} (\mathbf{c}_j \bar{\mathbf{c}}_j \partial_{\mathbf{c}_l} \partial_{\bar{\mathbf{c}}_l} + \mathbf{c}_l \bar{\mathbf{c}}_l \partial_{\mathbf{c}_j} \partial_{\bar{\mathbf{c}}_j} \\ &\quad - \mathbf{c}_j \mathbf{c}_l \partial_{\mathbf{c}_j} \partial_{\mathbf{c}_l} - \bar{\mathbf{c}}_j \bar{\mathbf{c}}_l \partial_{\bar{\mathbf{c}}_j} \partial_{\bar{\mathbf{c}}_l}), \\ \mathcal{L}_2 &= \frac{1}{2} \sum_{j,l=0}^{M-1} \Gamma_{jl}^{\text{D}} (\mathbf{c}_j \bar{\mathbf{c}}_l \partial_{\mathbf{c}_j} \partial_{\bar{\mathbf{c}}_l} + \bar{\mathbf{c}}_j \mathbf{c}_l \partial_{\bar{\mathbf{c}}_j} \partial_{\mathbf{c}_l} \\ &\quad - \mathbf{c}_j \mathbf{c}_l \partial_{\mathbf{c}_j} \partial_{\mathbf{c}_l} - \bar{\mathbf{c}}_j \bar{\mathbf{c}}_l \partial_{\bar{\mathbf{c}}_j} \partial_{\bar{\mathbf{c}}_l}), \end{aligned}$$

$$\mathcal{L}_3 = \frac{1}{2} \sum_{j=0}^{M-1} \Gamma_{jj}^{\text{OD}} (\mathbf{c}_j \partial_{\mathbf{c}_j} + \overline{\mathbf{c}_j} \partial_{\overline{\mathbf{c}_j}}) + i \hat{\Gamma}_{jj}^{\text{OD}} (\mathbf{c}_j \partial_{\mathbf{c}_j} - \overline{\mathbf{c}_j} \partial_{\overline{\mathbf{c}_j}}),$$

$$\mathcal{L}_4 = -\frac{1}{2} \sum_{j=0}^{M-1} \Gamma_{jj}^{\text{D}} (\mathbf{c}_j \partial_{\mathbf{c}_j} + \overline{\mathbf{c}_j} \partial_{\overline{\mathbf{c}_j}}),$$

$$\mathcal{L}_5 = i\gamma \sum_{l,m,n=0}^{M-1} \delta_{jlmn}^K Q_{jlmn} (\mathbf{c}_l \mathbf{c}_m \overline{\mathbf{c}_n} \partial_{\mathbf{c}_j} - \overline{\mathbf{c}_l} \mathbf{c}_m \mathbf{c}_n \partial_{\overline{\mathbf{c}_j}}),$$

where $\delta_{jlmn}^K = \mathbf{1}_{\beta_j - \beta_l - \beta_m + \beta_n = 0}$. In this definition we use the classical complex derivative: if $\zeta = \zeta_r + i\zeta_i$, then $\partial_\zeta = (1/2)(\partial_{\zeta_r} - i\partial_{\zeta_i})$ and $\partial_{\overline{\zeta}} = (1/2)(\partial_{\zeta_r} + i\partial_{\zeta_i})$, and the coefficients of the operator \mathcal{L}_k ($k = 1, \dots, 5$) are defined for $j, l = 0, \dots, M-1$, as follows:

- For all $j \neq l$, Γ_{jl} and $\hat{\Gamma}_{jl}^{\text{OD}}$ are given by

$$\Gamma_{jl}^{\text{OD}} = 2 \int_0^\infty \mathcal{R}_{jl}(z) \cos((\beta_l - \beta_j)z) dz, \quad (11)$$

$$\hat{\Gamma}_{jl}^{\text{OD}} = 2 \int_0^\infty \mathcal{R}_{jl}(z) \sin((\beta_l - \beta_j)z) dz, \quad (12)$$

with $\mathcal{R}_{jl}(z)$ defined by

$$\begin{aligned} \mathcal{R}_{jl}(z) &= \mathbb{E}[C_{jl}(0)C_{jl}(z)] \\ &= \iint u_j(\mathbf{r})u_j(\mathbf{r}') \mathbb{E}[\delta V(0, \mathbf{r})\delta V(z, \mathbf{r}')] u_l(\mathbf{r})u_l(\mathbf{r}') d\mathbf{r}d\mathbf{r}'. \end{aligned} \quad (13)$$

- For all $j, l = 0, \dots, M-1$:

$$\Gamma_{jl}^{\text{D}} = \int_0^\infty \mathbb{E}[C_{jj}(0)C_{ll}(z)] dz + \int_0^\infty \mathbb{E}[C_{ll}(0)C_{jj}(z)] dz. \quad (14)$$

- For all $j = 0, \dots, M-1$:

$$\Gamma_{jj}^{\text{OD}} = -\sum_{l=0, l \neq j}^{M-1} \Gamma_{jl}^{\text{OD}}, \quad \hat{\Gamma}_{jj}^{\text{OD}} = -\sum_{l=0, l \neq j}^{M-1} \hat{\Gamma}_{jl}^{\text{OD}}. \quad (15)$$

Secondary asymptotics

We observe that Γ^{OD} and $\hat{\Gamma}^{\text{OD}}$ depend on the power spectral density of the random index perturbation evaluated at the difference of distinct frequencies $\beta_j - \beta_l$, while Γ^{D} depends on the power spectral density of the index perturbation evaluated at zero-frequency. Therefore, when $L_{\text{lin}} = 1/\beta_0 \ll \ell_c$, then Γ^{D} is larger than $\Gamma^{\text{OD}}, \hat{\Gamma}^{\text{OD}}$. We consider this regime by introducing a small dimensionless parameter η with $\Gamma^{\text{D}} \rightarrow \Gamma^{\text{D}}, \Gamma^{\text{OD}} \rightarrow \eta^2 \Gamma^{\text{OD}}, \hat{\Gamma}^{\text{OD}} \rightarrow \eta^2 \hat{\Gamma}^{\text{OD}}, \gamma \rightarrow \eta\gamma$.

For propagation distances of order η^{-2} , we introduce the rescaled mode amplitudes $\mathbf{c}_j^\eta(z) = \mathbf{c}_j(z/\eta^2)$. By Proposition 1 it is a Markov process with infinitesimal generator \mathcal{L}^η :

$$\mathcal{L}^\eta = \mathcal{L}_1 + \eta^{-2} \mathcal{L}_2 + \mathcal{L}_3 + \eta^{-2} \mathcal{L}_4 + \eta^{-1} \mathcal{L}_5, \quad (16)$$

where the operators \mathcal{L}_k ($k = 1, \dots, 5$) are given above. By (16) the second-order moments satisfy for $j \neq j'$:

$$\begin{aligned} \partial_z \mathbb{E}[\mathbf{c}_j^\eta \overline{\mathbf{c}_{j'}^\eta}] &= -\frac{1}{2\eta^2} (\Gamma_{jj}^{\text{D}} + \Gamma_{j'j'}^{\text{D}} - 2\Gamma_{jj'}^{\text{D}}) \mathbb{E}[\mathbf{c}_j^\eta \overline{\mathbf{c}_{j'}^\eta}] \\ &\quad + \frac{1}{2} (\Gamma_{jj}^{\text{OD}} + \Gamma_{j'j'}^{\text{OD}}) \mathbb{E}[\mathbf{c}_j^\eta \overline{\mathbf{c}_{j'}^\eta}] + \frac{i}{2} (\hat{\Gamma}_{jj}^{\text{OD}} - \hat{\Gamma}_{j'j'}^{\text{OD}}) \mathbb{E}[\mathbf{c}_j^\eta \overline{\mathbf{c}_{j'}^\eta}] \\ &\quad + i\frac{\gamma}{\eta} \sum_{l,m,n=0}^{M-1} \delta_{jlmn}^K Q_{jlmn} \mathbb{E}[\mathbf{c}_j^\eta \mathbf{c}_l^\eta \overline{\mathbf{c}_m^\eta} \overline{\mathbf{c}_n^\eta}] \\ &\quad - i\frac{\gamma}{\eta} \sum_{l,m,n=0}^{M-1} \delta_{j'lmn}^K Q_{j'lmn} \mathbb{E}[\mathbf{c}_{j'}^\eta \mathbf{c}_l^\eta \overline{\mathbf{c}_m^\eta} \overline{\mathbf{c}_n^\eta}], \end{aligned}$$

up to negligible terms in η . Note that $\Gamma_{jj}^{\text{D}} + \Gamma_{j'j'}^{\text{D}} - 2\Gamma_{jj'}^{\text{D}} = \int_{-\infty}^\infty \mathbb{E}[(C_{jj}(0) - C_{j'j'}(0))(C_{jj}(z) - C_{j'j'}(z))] dz$ is positive (it is the power spectral density evaluated at 0 frequency of the stationary process $C_{jj}(z) - C_{j'j'}(z)$ by Bochner's theorem). Therefore $\mathbb{E}[\mathbf{c}_j^\eta \overline{\mathbf{c}_{j'}^\eta}]$ is exponentially damped and

$$\mathbb{E}[\mathbf{c}_j^\eta \overline{\mathbf{c}_{j'}^\eta}] = O(\eta). \quad (17)$$

If $j = j'$, then the mean square amplitudes $w_j^\eta(z) = \mathbb{E}[|\mathbf{c}_j^\eta(z)|^2]$ satisfy

$$\begin{aligned} \partial_z w_j^\eta &= \sum_{l=0, l \neq j}^{M-1} \Gamma_{jl}^{\text{OD}} (w_l^\eta - w_j^\eta) \\ &\quad - 2\frac{\gamma}{\eta} \sum_{l,m,n=0}^{M-1} \delta_{jlmn}^K Q_{jlmn} \text{Im}\left\{ \mathbb{E}[\overline{\mathbf{c}_j^\eta} \mathbf{c}_l^\eta \overline{\mathbf{c}_m^\eta} \mathbf{c}_n^\eta] \right\}. \end{aligned} \quad (18)$$

By (16) the fourth-order moments satisfy

$$\begin{aligned} \partial_z \mathbb{E}[\overline{\mathbf{c}_j^\eta} \mathbf{c}_l^\eta \overline{\mathbf{c}_m^\eta} \mathbf{c}_n^\eta] &= -\frac{1}{2\eta^2} G_{jlmn}^{\text{D}} \mathbb{E}[\overline{\mathbf{c}_j^\eta} \mathbf{c}_l^\eta \overline{\mathbf{c}_m^\eta} \mathbf{c}_n^\eta] + i\frac{\gamma}{\eta} Y_{jlmn}^\eta \\ &\quad + \sum_{j', l', m', n'} M_{jlmn, j' l' m' n'} \mathbb{E}[\overline{\mathbf{c}_j^\eta} \mathbf{c}_{l'}^\eta \overline{\mathbf{c}_{m'}^\eta} \mathbf{c}_{n'}^\eta], \end{aligned} \quad (19)$$

up to negligible terms in η . The coefficients G_{jlmn}^{D} and the sixth-order moment Y_{jlmn}^η are given by

$$\begin{aligned} G_{jlmn}^{\text{D}} &= \Gamma_{ll}^{\text{D}} + \Gamma_{mm}^{\text{D}} + \Gamma_{nn}^{\text{D}} + \Gamma_{jj}^{\text{D}} + 2\Gamma_{lm}^{\text{D}} - 2\Gamma_{ln}^{\text{D}} \\ &\quad - 2\Gamma_{lj}^{\text{D}} - 2\Gamma_{mn}^{\text{D}} - 2\Gamma_{mj}^{\text{D}} + 2\Gamma_{nj}^{\text{D}}, \end{aligned} \quad (20)$$

$$\begin{aligned} Y_{jlmn}^\eta &= \sum_{l', m', n'=0}^{M-1} \delta_{ll'm'n'}^K S_{ll'm'n'} \mathbb{E}[\mathbf{c}_l^\eta \mathbf{c}_{l'}^\eta \overline{\mathbf{c}_m^\eta} \overline{\mathbf{c}_{m'}^\eta} \mathbf{c}_n^\eta \overline{\mathbf{c}_{n'}^\eta}] \\ &\quad + \delta_{ml'm'n'}^K S_{ml'm'n'} \mathbb{E}[\mathbf{c}_l^\eta \mathbf{c}_{l'}^\eta \mathbf{c}_m^\eta \overline{\mathbf{c}_{m'}^\eta} \overline{\mathbf{c}_n^\eta} \overline{\mathbf{c}_{n'}^\eta}] \\ &\quad - \delta_{nl'm'n'}^K S_{nl'm'n'} \mathbb{E}[\mathbf{c}_l^\eta \mathbf{c}_m^\eta \overline{\mathbf{c}_{l'}^\eta} \overline{\mathbf{c}_m^\eta} \mathbf{c}_{n'}^\eta \overline{\mathbf{c}_j^\eta}] \\ &\quad - \delta_{jl'm'n'}^K Q_{jl'm'n'} \mathbb{E}[\mathbf{c}_l^\eta \mathbf{c}_m^\eta \overline{\mathbf{c}_{l'}^\eta} \overline{\mathbf{c}_m^\eta} \mathbf{c}_{n'}^\eta], \end{aligned} \quad (21)$$

up to negligible terms in η . The tensor $M_{jlmn, j' l' m' n'}$ involves the coefficients Γ^{OD} and $\hat{\Gamma}^{\text{OD}}$. Note that we

have $G_{jlmn}^D = \int_{-\infty}^{\infty} \mathbb{E}[(C_{ll}(0) + C_{mm}(0) - C_{nn}(0) - C_{jj}(0))(C_{ll}(z) + C_{mm}(z) - C_{nn}(z) - C_{jj}(z))]dz \geq 0$. Therefore, we find from (19) that

$$\mathbb{E}[\bar{\mathbf{c}}_j^\eta \mathbf{c}_l^\eta \bar{\mathbf{c}}_m^\eta \mathbf{c}_n^\eta] = \frac{2i\eta\gamma}{G_{jlmn}^D} Y_{jlmn}^\eta + O(\eta^2).$$

By substituting into (18) and by using Isserlis formula for the sixth-order moments that appear in the expression (21) of Y_{jlmn}^η we obtain the kinetic Eq.(4):

$$\begin{aligned} \partial_z w_j^\eta &= \sum_{l=0, l \neq j}^{M-1} \Gamma_{jl}^{\text{OD}} (w_l^\eta - w_j^\eta) \\ &+ 8\gamma^2 \sum_{l,m,n=0}^{M-1} \frac{\delta_{jlmn}^K Q_{jlmn}^2}{G_{jlmn}^D} (w_l^\eta w_m^\eta w_j^\eta + w_l^\eta w_m^\eta w_n^\eta \\ &\quad - w_j^\eta w_n^\eta w_m^\eta - w_j^\eta w_n^\eta w_l^\eta). \end{aligned} \quad (22)$$

The second term in (22) has a form analogous to the conventional collision term of the wave turbulence kinetic equation [1]. Exploiting the invariances properties of the tensors Q_{jlmn} and G_{jlmn}^D , as well as the property $G_{jlmn}^D \geq 0$, it can be shown that the collision term conserves the particle number $N = \sum_j w_j$, the energy $E = \sum_j \beta_j w_j$, and exhibits a H -theorem of entropy growth $\partial_z S(z) \geq 0$, where the nonequilibrium entropy reads $S(z) = \sum_j \log[w_j(z)]$ (note that, for simplicity we omitted to write the superscript η). The entropy growth saturates at thermal equilibrium. The RJ equilibrium distribution that maximizes the entropy $S[w_j]$, under the constraints that N and E are conserved, reads

$$w_j^{\text{RJ}} = T/(\beta_j - \mu), \quad (23)$$

where $1/T$ and $-\mu/T$ are the Lagrange multipliers associated to the conservation of E and N . There is a one to one relation between the pair (N, E) and (T, μ) : The values of the conserved quantities (N, E) determine uniquely (T, μ) , and thus the RJ equilibrium (23).

Degenerate modes

In this section we assume that the modes may be degenerate. The detailed derivation of the kinetic equation accounting for mode degeneracy is cumbersome and will be reported elsewhere. Here we report the main results.

There are G distinct wavenumbers:

$$\{\beta^{(g)}, g = 1, \dots, G\},$$

and the mode indices can be partitioned into G groups $\mathcal{G}^{(g)}, g = 1, \dots, G$:

$$\mathcal{G}^{(g)} = \{p = 1, \dots, N, \beta_p = \beta^{(g)}\}.$$

We obtain the kinetic equation

$$\begin{aligned} \partial_z w^{(g)} &= 8\gamma^2 \sum_{g_1, g_2, g_3=1}^G \delta^{(gg_1 g_2 g_3)} q^{(gg_1 g_2 g_3)} (w^{(g)} w^{(g_3)} w^{(g_2)} \\ &\quad + w^{(g)} w^{(g_3)} w^{(g_1)} - w^{(g_1)} w^{(g_2)} w^{(g)} - w^{(g_1)} w^{(g_2)} w^{(g_3)}), \end{aligned}$$

where

$$q^{(gg_1 g_2 g_3)} = \frac{1}{|\mathcal{G}^{(g)}|} \sum_{j \in \mathcal{G}^{(g)}, l \in \mathcal{G}^{(g_1)}, m \in \mathcal{G}^{(g_2)}, n \in \mathcal{G}^{(g_3)}} Q_{jlmn} Q_{jlmn}^{(gg_1 g_2 g_3)}$$

where

$$\begin{aligned} Q^{(gg_1 g_2 g_3)} &= (Q_{jlmn}^{(gg_1 g_2 g_3)})_{j \in \mathcal{G}^{(g)}, l \in \mathcal{G}^{(g_1)}, m \in \mathcal{G}^{(g_2)}, n \in \mathcal{G}^{(g_3)}} \\ &= (\mathbf{M}^{(gg_1 g_2 g_3)})^{-1} ((Q_{jlmn})_{j \in \mathcal{G}^{(g)}, l \in \mathcal{G}^{(g_1)}, m \in \mathcal{G}^{(g_2)}, n \in \mathcal{G}^{(g_3)}}). \end{aligned}$$

The tensor $\mathbf{M}^{(gg_1 g_2 g_3)}$ (seen as a $q \times q$ matrix with $q = |\mathcal{G}^{(g)}| |\mathcal{G}^{(g_1)}| |\mathcal{G}^{(g_2)}| |\mathcal{G}^{(g_3)}|$) is given by

$$\begin{aligned} &\sum_{j' \in \mathcal{G}^{(g)}, l' \in \mathcal{G}^{(g_1)}, m' \in \mathcal{G}^{(g_2)}, n' \in \mathcal{G}^{(g_3)}} M_{jlmn, j'l'm'n'}^{(gg_1 g_2 g_3)} w_{j'l'm'n'} \\ &= \sum_{l' \in \mathcal{G}^{(g_1)}, m' \in \mathcal{G}^{(g_2)}} 2\gamma_{ll'mm'} w_{jl'm'n} \\ &\quad + \sum_{n' \in \mathcal{G}^{(g_3)}, j' \in \mathcal{G}^{(g)}} 2\gamma_{nn'jj'} w_{jl'mn'} \\ &\quad - \sum_{l' \in \mathcal{G}^{(g_1)}, n' \in \mathcal{G}^{(g_3)}} 2\gamma_{ll'nn'} w_{jl'mn'} \\ &\quad - \sum_{l' \in \mathcal{G}^{(g_1)}, j' \in \mathcal{G}^{(g)}} 2\gamma_{ll'jj'} w_{jl'l'mn} \\ &\quad - \sum_{m' \in \mathcal{G}^{(g_2)}, n' \in \mathcal{G}^{(g_3)}} 2\gamma_{mm'nn'} w_{jlm'n'} \\ &\quad - \sum_{m' \in \mathcal{G}^{(g_2)}, j' \in \mathcal{G}^{(g)}} 2\gamma_{mm'jj'} w_{jl'm'n} \\ &\quad + \sum_{l', l'' \in \mathcal{G}^{(g_1)}} \gamma_{l'l''} w_{jl'l'mn} + \sum_{m', m'' \in \mathcal{G}^{(g_2)}} \gamma_{m'm''} w_{jlm'n} \\ &\quad + \sum_{n', n'' \in \mathcal{G}^{(g_3)}} \gamma_{n'n''} w_{jlmn'} + \sum_{j', j'' \in \mathcal{G}^{(g)}} \gamma_{j'j''} w_{jl'mn}. \end{aligned}$$

where

$$\gamma_{pp'q'q'} = 2 \int_0^\infty \mathbb{E}[C_{pq}(z) C_{p'q'}(0)] e^{i(\beta_p - \beta_{q'})z} dz.$$

Numerical simulations

Implementation of disorder: To implement the disorder in the simulations of the NLS Eq.(2), we considered an *exact discretization* of the Ornstein-Uhlenbeck process. The propagation axis is divided in intervals with deterministic lengths Δz , with $\Delta z < \ell_c$. The random function $\mu(z)$ is stepwise constant over each elementary interval

$z \in [k\Delta z, (k+1)\Delta z]$, where $\mu_0 \sim \mathcal{N}(0, \sigma^2/2)$ denotes the Gaussian distribution, $\mu_k = \sqrt{1 - 2\Delta z/\ell_c} \mu_{k-1} + \sqrt{2\Delta z/\ell_c} \mathcal{N}(0, \sigma^2/2)$, with $\mathcal{N}(0, \sigma^2/2)$ all independent and identically distributed.

Model of disorder: We have considered in the numerical simulations an elliptical parabolic potential $V(\mathbf{x}) = q_x x^2 + q_y y^2$, with $u_{p_x, p_y}(x, y) = \sqrt{\kappa_x \kappa_y} (\pi p_x! p_y! 2^{p_x+p_y})^{-1/2} H_{p_x}(\kappa_x x) H_{p_y}(\kappa_y y) \exp[-(\kappa_x^2 x^2 + \kappa_y^2 y^2)/2]$ the normalized Hermite-Gaussian functions with corresponding eigenvalues $\beta_p = \beta_{p_x, p_y} = \beta_{0x}(p_x + 1/2) + \beta_{0y}(p_y + 1/2)$, with $\kappa_x = (q_x/\alpha)^{1/4}$, $\kappa_y = (q_y/\alpha)^{1/4}$, $\beta_{0x} = 2\sqrt{\alpha q_x}$, $\beta_{0y} = 2\sqrt{\alpha q_y}$, and the radii of the fundamental mode $r_{0x} = 1/\kappa_x = \sqrt{2\alpha/\beta_{0x}}$, $r_{0y} = 1/\kappa_y = \sqrt{2\alpha/\beta_{0y}}$.

We have considered the following form of model of disorder: $\delta V(\mathbf{x}, z) = \mu(z) \cos(\kappa_x b_x x) \cos(\kappa_y b_y y)$, with $\mathbb{E}[\mu(0)\mu(z)] = \sigma^2 f(z)$, $f(z) = \exp(-|z|/\ell_c)$. The advantage of this model is that the matrices $\mathbf{C}, \mathbf{\Gamma}^D, \mathbf{\Gamma}^{OD}$ can be computed in analytical form. We have $C_{nk}(z) = \mu(z) C_{n_x k_x}^0 C_{n_y k_y}^0 = \mu(z) \int u_{n_x}(x) \cos(\kappa_x b_x x) u_{k_x}(x) dx \times \int u_{n_y}(y) \cos(\kappa_y b_y y) u_{k_y}(y) dy$. Then we have for $j_x, j_y, l_x, l_y \geq 0$: $C_{j, j+2l} = \mu(z) C_{j_x, j_x+2l_x}^0 C_{j_y, j_y+2l_y}^0$ where we denote for $s = x$ or $s = y$:

$$C_{j_s, j_s+2l_s}^0 = (-1)^{l_s} b_s^{2l_s} \exp(-b_s^2/4) \times L_{j_s}^{2l_s} (b_s^2/2) \frac{\sqrt{j_s!/(j_s+2l_s)!}}{2^{l_s}}$$

and $C_{j_s, j_s+2l_s+1}^0 = 0$, where L_j^l is the generalized Laguerre polynomial [56, formula 7.388.7]. In particular $C_{j_s j_s}^0 = \exp(-b_s^2/4) L_{j_s}^0(b_s^2/2)$, where L_j is the Laguerre polynomial. For $j_x, j_y, l_x, l_y \geq 0$, we have $\Gamma_{jl}^D = 2\sigma^2 \ell_c C_{j_x j_x}^0 C_{j_y j_y}^0 C_{l_x l_x}^0 C_{l_y l_y}^0$. For $n_x, k_x, n_y, k_y \geq 0$ we obtain:

$$\Gamma_{n,k}^{OD} = \frac{2\sigma^2 \ell_c \mathcal{R}_{n_x, k_x}^0 \mathcal{R}_{n_y, k_y}^0}{1 + \ell_c^2 [\beta_{0x}(n_x - k_x) + \beta_{0y}(n_y - k_y)]^2},$$

where $\mathcal{R}_{j_s, j_s+2l_s+1}^0 = 0$ and

$$\mathcal{R}_{j_s, j_s+2l_s}^0 = b_s^{4l_s} \exp(-b_s^2/2) L_{j_s}^{2l_s} (b_s^2/2)^2 (j_s!/(j_s+2l_s)!) 2^{-2l_s}.$$

In order to avoid high values of $\Gamma_{n,k}^{OD}$, we have considered an irrational ratio $\beta_{0x}/\beta_{0y} = \sqrt{2}$, so that $\beta_{0x}(n_x - k_x) + \beta_{0y}(n_y - k_y) \neq 0$. Parameters are $(b_x = 0.4, b_y = 0.5)$ in Figs. 1-2, and $(b_x = 0.4, b_y = 0.3)$ in Fig. 3. In all cases we considered $M = 46$ modes. The value of $L_{nl} = 1/(\gamma N/A_{eff}^0)$ in the simulations is computed by considering that all the power N is in the fundamental mode of effective area $A_{eff}^0 = 1/\int |u_0|^4(\mathbf{r}) d\mathbf{r}$.

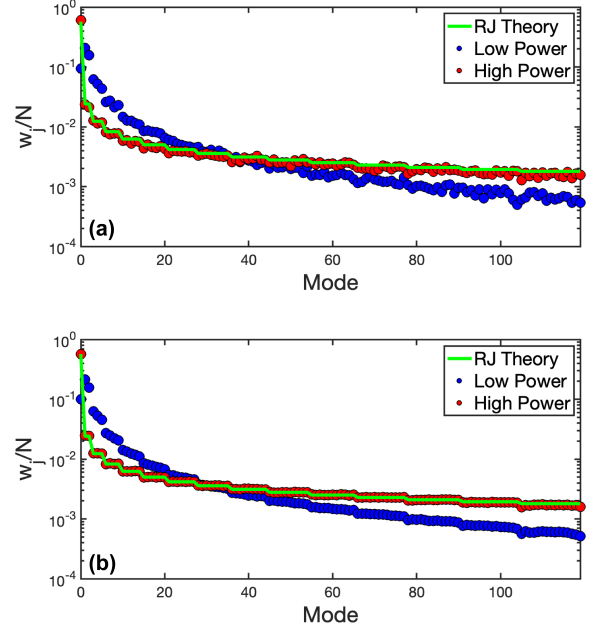


FIG. 5: **Observation of RJ thermalization (without disorder):** Experimental modal distributions w_j/N (circles), for an individual realization of the launched speckle beam (a), for an average over the realizations of speckle beams (b). The red circles report the results at high power ($N = 7\text{kW}$, nonlinear regime), and the blue circles at low power ($N = 0.23\text{kW}$, linear regime). The condensate fraction is $w_0/N = 0.6$ for $E/N = 1.94 \times 10^4 \text{m}^{-1}$ (a); $w_0/N = 0.57$ for $E/N = 2.05 \times 10^4 \text{m}^{-1}$ (b). Corresponding theoretical RJ equilibrium distribution w_j^{RJ}/N given from Eq.(23) (green line): The quantitative agreement with the experimental data (red circles) is obtained without using any adjustable parameter.

EXPERIMENTAL METHODS

1) Setup: The experimental setup has been described in detail in Ref.[29]. Here we summarize the main characteristics. The source is a Nd:YAG laser delivering sub-nanosecond pulses (400ps) at $\lambda_0 = 1064 \text{nm}$. We control the power with a half-wave plate and a polarizer. The laser beam was collimated and passed through a glass diffuser plate placed in the vicinity of the Fourier plane of a 4f-optical system. The beam was launched into the MMF. The near-field (NF) and far-field (FF) intensity distributions are measured at the fiber output following the procedure of Ref.[29]. We used a 12m-long graded-index MMF whose refractive index profile exhibits a parabolic shape in the fiber core with a maximum core index (at the center) of $n_{\text{co}} = 1.470$ and $n_{\text{cl}} = 1.457$ for the cladding at the pump wavelength of 1064nm (numerical aperture $\text{NA} = 0.195$, fiber radius $R = 26 \mu\text{m}$, $\beta_0 \simeq 5 \times 10^3 \text{m}^{-1}$). The MMF guides $M \simeq 120$ modes. The truncation of the potential introduces a frequency cut-off in the FF spectrum $k_c = (2\pi/\lambda_0) \sqrt{n_{\text{co}}^2 - n_{\text{cl}}^2}$. For details, see Supplementary Methods in Ref.[29].

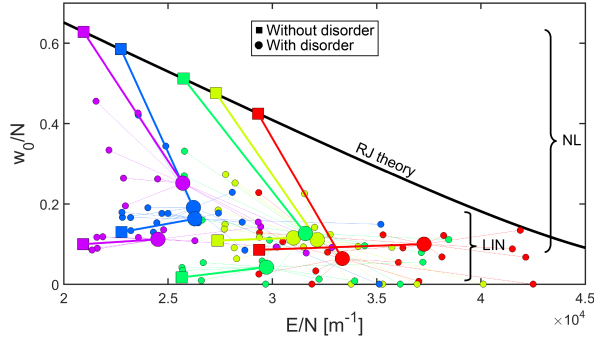


FIG. 6: Suppression of light thermalization and condensation by strong disorder: Measurements of the condensate fraction w_0/N vs energy E/N at small power (linear (LIN) regime) and high power (nonlinear (NL) regime), for a large strength of random mode coupling corresponding to an increase of the energy due to disorder of $\Delta E/N \simeq 19\%$. The black solid line reports the condensate fraction from the RJ theory, w_0^{RJ}/N vs E/N . In the absence of strong disorder (squares): w_0/N increases as the power increases, and reaches the value predicted by the RJ theory (solid line) – each color refers to a different value of the energy E/N . In the presence of strong disorder (big circles): the energy E/N increases (the squares are shifted to the big circles of the same color). The big circles report the average over 10 different realizations of disorder (10 small circles for each color). At variance with Fig. 4, here the strength of random mode coupling is so large that RJ thermalization and condensation are inhibited by strong disorder.

The temporal spectrum was controlled by an optical spectrum analyzer (OSA) (600 to 1700nm range). The spectral analysis showed that the power scattered by self-stimulated Raman effect is in average $\sim 5\%$ of the injected power. Also, the spectral analysis did not reveal the presence of parametric lines that would be induced by coupling between dispersive and nonlinear effects.

2) Conservation of power N and energy E during propagation without strong disorder: The conservation of the power has been verified by keeping fixed the conditions of injection of the speckle beam into the MMF: We measured N at the fiber output, and then at the input by cutting the fiber at 20cm, and we always obtained a relative power difference less than 1%. The conservation of the energy requires the NF and FF intensity measurements, which provide the potential energy $E_{\text{pot}} = \int V(\mathbf{r})|\psi(\mathbf{r})|^2 d\mathbf{r}$, and the kinetic energy $E_{\text{kin}} = \int \alpha |\nabla \psi|^2 d\mathbf{r}$, with $E = E_{\text{kin}} + E_{\text{pot}}$. The energy E_{out} is measured at the fiber output at $L = 12\text{m}$. Without altering the fiber launch conditions, the fiber is cut to 20cm to get E_{in} . The procedure is repeated for different speckle beams (i.e., for different values of the energy E), by moving the diffuser before injection into the MMF. We always obtained $|E_{\text{out}} - E_{\text{in}}|/E_{\text{moy}} < 1\%$ for values of the energy that span the range of the condensation curve, i.e. w_0^{RJ}/N varying from 0 to 0.7.

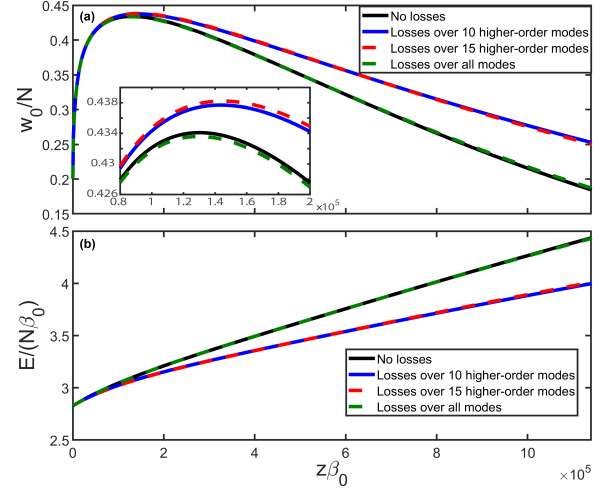


FIG. 7: Impact of losses on the condensate fraction: Simulation of the kinetic Eq.(22) for the same parameters as Fig. 2: In the absence of losses (black), and when 10% of losses are distributed among all modes (dashed green), among the higher-order 10 modes of the fiber (blue), among the higher-order 15 modes of the fiber (dashed red). Condensate fraction $w_0(z)/N(z)$ vs z , where $N(z)$ is the local value of the power accounting for the losses (a), and corresponding evolutions of the energy $E(z)/(N(z)\beta_0)$ (b). The inset in (a) shows a zoom: The condensate peak relevant to the experiments is only weakly affected by the presence of the losses.

3) Experimental observation of RJ thermalization: In the absence of strong disorder (i.e., absence of applied stress induced on the fiber), we observe the process of thermalization to the RJ equilibrium distribution, $w_j^{\text{RJ}} = T/(\beta_j - \mu)$. In the experiments, the modal populations (w_j) are computed by using the Gerchberg-Saxton algorithm, which allows us to retrieve the transverse phase profile of the field from the NF and the FF intensity distributions measured in the experiments [57]. By projecting the complex field over the modes of the MMF (Gauss-Hermite basis) we get the complete modal distribution w_j/N , $j = 0, 1, \dots, M-1$. A typical example is reported in Fig. 5 showing the modal distribution w_j/N recorded experimentally at low-power (linear regime) and high-power (nonlinear regime), and its comparison to the RJ equilibrium distribution. Fig. 5(a) reports a single realization of the speckle beam, Fig. 5(b) reports an average over 60 realizations of speckle beams. The quantitative agreement between the experimental results and the theoretical RJ distribution is obtained without using adjustable parameters.

4) Experimental procedure with strong disorder (applied stress): The laser beam is passed through a diffuser before injection of the speckle beam into the MMF. The coupling conditions and the position of the diffuser then fix the energy density E/N of the speckle beam. In the absence of applied stress, E/N is conserved through propagation in the MMF (see point 2) above).

We report in Fig. 4(a), 5 different ensembles of measurements, each one corresponding to a fixed position of the diffuser (i.e. fixed value of the energy E/N without applied stress). For a given fixed position of the diffuser, we perform the following steps i)-vii) to retrieve 10 different realizations of disorder in Fig. 4(a):

- i) Without applying any stress, we measure the NF and FF intensity patterns at high power ($N = 7\text{kW}$, nonlinear regime), and compute E/N and w_0/N (squares in Fig. 4(a)). We verify that w_0/N is in agreement with the value predicted by the RJ theory, see Ref.[29] for details.
- ii) At low power ($N = 0.23\text{kW}$, linear regime) we measure the NF and FF intensity patterns and compute E/N and w_0/N .
- iii) We return to the previous higher power ($N = 7\text{kW}$, nonlinear regime) and we verify that we recover the same NF speckle beam as in step i).
- iv) Then we apply stress to a specific location of the MMF. The stress is applied by using clamps mounted on a linear translation manual stage whose position is controlled at the micrometer scale. We adjust the amount of stress by measuring the power losses (10% in Fig. 4(a), corresponding to $\Delta E/N \simeq 6\%$). Once the stress is adjusted, the power is increased up to the same average power of step i). We then measure the NF and FF intensity patterns and compute E/N and w_0/N (small circles in Fig. 4(a)).
- v) In a next step we decrease the power ($N = 0.23\text{kW}$, linear regime), we measure the NF and FF intensity patterns and compute E/N and w_0/N (small circles in Fig. 4(a)).
- vi) We return to the previous higher power ($N = 7\text{kW}$, nonlinear regime) and remove the applied stress. We verify that we recover the same initial NF speckle beam as in step i).
- vii) We repeat the steps iv)-v)-vi) 10 times to get 10 different realizations of strong disorder (small circles). Each disorder realization is achieved by applying stress to a different position of the MMF by rotating the drum on which it is wound.

The procedure i)-vii) is repeated for a larger amount of applied stress (disorder), corresponding to an increase of energy due to disorder of $\Delta E/N \simeq 11\%$ in Fig. 4(b) (20% of power losses), and $\Delta E/N \simeq 19\%$ in Fig. 6 (40% of power losses). In Fig. 6 the strength of random mode coupling is so large that RJ thermalization and condensation are inhibited by strong disorder.

Note that losses induced by strong disorder only weakly affect the condensate fraction through the propagation in the MMF, as illustrated in the simulation reported in Fig. 7. We have considered 10% of losses (over the propagation length $z\beta_0 = 11 \times 10^5$), in the case where losses are distributed homogeneously in mode space, and non-homogeneously in mode space (only the higher-order modes experience losses). We have considered the param-

eters of the simulation reported in Fig. 2, which refers to the most interesting regime where linear disorder effects and nonlinear effects are of the same order, $\mathcal{L}_{\text{kin}}^{\text{RJ}} \lesssim \mathcal{L}_{\text{kin}}^{\text{eq}}$. The condensate peak relevant to the experiments is only weakly affected by the losses, see the inset in Fig. 7(a). Note that, for larger propagation lengths, the losses concentrated on the higher-order modes reduce the effective number of modes and thus limit the increase of energy $E/(N\beta_0)$ due to disorder (Fig. 7(b)), which in turn leads to an increase of the condensate fraction (Fig. 7(a)).

-
- [1] V.E. Zakharov, V.S. L'vov, G. Falkovich, *Kolmogorov Spectra of Turbulence I* (Springer, Berlin, 1992).
 - [2] A.C. Newell, S. Nazarenko, L. Biven, Wave turbulence and intermittency, *Physica D* **152**, 520 (2001).
 - [3] S. Nazarenko, *Wave Turbulence* (Springer, Lectures Notes in Physics, 2011).
 - [4] A.C. Newell, B. Rumpf, Wave Turbulence, *Annu. Rev. Fluid Mech.* **43**, 59 (2011).
 - [5] *Advances in Wave Turbulence*, World Scientific Series on Nonlinear Science Series A, Vol. 83, edited by V.I. Shrira (World Scientific, Singapore, 2013).
 - [6] J. Laurie, U. Bortolozzo, S. Nazarenko, S. Residori, One-dimensional optical wave turbulence: experiment and theory, *Physics Reports* **514**, 121-175 (2012).
 - [7] V.S. L'vov, S.V. Nazarenko, Discrete and mesoscopic regimes of finite-size wave turbulence, *Phys. Rev. E* **82**, 056322 (2010).
 - [8] M. Onorato, L. Vozella, D. Proment, and Y.V. L'vov, Route to thermalization in the α -Fermi-Pasta-Ulam system, *Proc. Natl. Acad. Sci. (PNAS)* **112**, 4208 (2015).
 - [9] A. Picozzi, J. Garnier, T. Hansson, P. Suret, S. Randoux, G. Millot, D.N. Christodoulides, Optical wave turbulence: Toward a unified nonequilibrium thermodynamic formulation of statistical nonlinear optics, *Physics Reports* **542**, 1-132 (2014).
 - [10] C. Connaughton, C. Josserand, A. Picozzi, Y. Pomeau, S. Rica, Condensation of classical nonlinear waves, *Phys. Rev. Lett.* **95**, 263901 (2005).
 - [11] N.G. Berloff, A.J. Youd, Dissipative dynamics of superfluid vortices at nonzero temperatures, *Phys. Rev. Lett.* **99**, 145301 (2007).
 - [12] G. Düring, A. Picozzi, S. Rica, Breakdown of weak-turbulence and nonlinear wave condensation, *Physica D* **238**, 1524 (2009).
 - [13] G. Krstulovic, M. Brachet, Energy cascade with small-scale thermalization, counterflow metastability, and anomalous velocity of vortex rings in Fourier-truncated Gross-Pitaevskii equation, *Phys. Rev. E* **83**, 066311 (2011).
 - [14] S. Nazarenko, M. Onorato, D. Proment, Bose-Einstein condensation and Berezinskii-Kosterlitz-Thouless transition in the two-dimensional nonlinear Schrödinger model, *Phys. Rev. A* **90**, 013624 (2014).
 - [15] A. Rückriegel, P. Kopietz, Rayleigh-Jeans condensation of pumped magnons in thin-film ferromagnets, *Phys. Rev. Lett.* **115**, 157203 (2015).
 - [16] A. Chiochetta, P.E. Larré, I. Carusotto, Thermalization and Bose-Einstein condensation of quantum light in bulk

- nonlinear media, *Europhys. Lett.* **115**, 24002 (2016).
- [17] N. Santic, A. Fusaro, S. Salem, J. Garnier, A. Picozzi, R. Kaiser, Nonequilibrium precondensation of classical waves in two dimensions propagating through atomic vapors, *Phys. Rev. Lett.* **120**, 055301 (2018).
 - [18] J. Bloch, I. Carusotto, M. Wouters, Spontaneous coherence in spatially extended photonic systems: Non-Equilibrium Bose-Einstein condensation, arXiv:2106.11137 (2021) – to be published in *Nature Reviews Physics*.
 - [19] K. Krupa, A. Tonello, A. Barthélémy, V. Couderc, B.M. Shalaby, A. Bendahmane, G. Millot, S. Wabnitz, Observation of geometric parametric instability induced by the periodic spatial self-imaging of multimode waves, *Phys. Rev. Lett.* **116**, 183901 (2016).
 - [20] L.G. Wright, Z. Liu, D.A. Nolan, M.-J. Li, D.N. Christodoulides, F.W. Wise, Self-organized instability in graded-index multimode fibres, *Nature Photon.* **10**, 771 (2016).
 - [21] K. Krupa, A. Tonello, B.M. Shalaby, M. Fabert, A. Barthélémy, G. Millot, S. Wabnitz, V. Couderc, Spatial beam self-cleaning in multimode fibres, *Nature Photon.* **11**, 237 (2017).
 - [22] P. Aschieri, J. Garnier, C. Michel, V. Doya, A. Picozzi, Condensation and thermalization of classical optical waves in a waveguide, *Phys. Rev. A* **83**, 033838 (2011).
 - [23] A. Fusaro, J. Garnier, K. Krupa, G. Millot, A. Picozzi, Dramatic acceleration of wave condensation mediated by disorder in multimode fibers, *Phys. Rev. Lett.* **122**, 123902 (2019).
 - [24] E. Podivilov, D. Kharenko, V. Gonta, K. Krupa, O.S. Sidelnikov, S. Turitsyn, M.P. Fedoruk, S.A. Babin, S. Wabnitz, Hydrodynamic 2D turbulence and spatial beam condensation in multimode optical fibers, *Phys. Rev. Lett.* **122**, 103902 (2019).
 - [25] J. Garnier, A. Fusaro, K. Baudin, C. Michel, K. Krupa, G. Millot, A. Picozzi, Wave condensation with weak disorder versus beam self-cleaning in multimode fibers, *Phys. Rev. A* **100**, 053835 (2019).
 - [26] F.O. Wu, A.U. Hassan, D.N. Christodoulides, Thermodynamic theory of highly multimoded nonlinear optical systems, *Nature Photon.* **13**, 776 (2019).
 - [27] A. Ramos, L. Fernández-Alcázar, T. Kottos, B. Shapiro, Optical Phase Transitions in Photonic Networks: a Spin-System Formulation *Phys. Rev. X* **10**, 031024 (2020).
 - [28] F.O. Wu, Q. Zhong, H. Ren, P.S. Jung, K.G. Makris, D.N. Christodoulides, Thermalization of Light's Orbital Angular Momentum in Nonlinear Multimode Waveguide Systems, *Phys. Rev. Lett.* **128**, 123901 (2022).
 - [29] K. Baudin, A. Fusaro, K. Krupa, J. Garnier, S. Rica, G. Millot, A. Picozzi, Classical Rayleigh-Jeans condensation of light waves: Observation and thermodynamic characterization, *Phys. Rev. Lett.* **125**, 244101 (2020).
 - [30] H. Pourbeyram, P. Sidorenko, F. Wu, L. Wright, D. Christodoulides, F. Wise, Direct measurement of thermalization to Rayleigh-Jeans distribution in optical beam self cleaning, *Nature Physics* **18**, 685 (2022).
 - [31] K. Baudin, A. Fusaro, J. Garnier, N. Berti, K. Krupa, I. Carusotto, S. Rica, G. Millot, A. Picozzi, Energy and wave-action flows underlying Rayleigh-Jeans thermalization of optical waves propagating in a multimode fiber, *Europhys. Lett.* **134**, 14001 (2021).
 - [32] F. Mangini, M. Gervaziev, M. Ferraro, D. S. Kharenko, M. Zitelli, Y. Sun, V. Couderc, E.V. Podivilov, S.A. Babin, and S. Wabnitz, Statistical mechanics of beam self-cleaning in GRIN multimode optical fibers, *Opt. Exp.* **30**, 10850 (2022).
 - [33] E.V. Podivilov, F. Mangini, O.S. Sidelnikov, M. Ferraro, M. Gervaziev, D.S. Kharenko, M. Zitelli, M.P. Fedoruk, S.A. Babin, S. Wabnitz, Thermalization of orbital angular momentum beams in multimode optical fibers, *Phys. Rev. Lett.* **128**, 243901 (2022).
 - [34] C. Conti, E. DelRe, Photonics and the Nobel Prize in Physics, *Nature Photonics* **16**, 6 (2022).
 - [35] D. Pierangeli, A. Tavani, F. Di Mei, A.J. Agranat, C. Conti, E. DelRe, Observation of replica symmetry breaking in disordered nonlinear wave propagation, *Nature Commun.* **8**, 1501 (2017).
 - [36] D. Churkin, I. Kolokolov, E. Podivilov, I. Vatik, S. Vergeles, I. Terekhov, V. Lebedev, G. Falkovich, M. Nikulin, S. Babin, S. Turitsyn, Wave kinetics of a random fibre laser, *Nature Commun.* **2**, 6214 (2015).
 - [37] M. Segev, Y. Silberberg, D.N. Christodoulides, Anderson localization of light, *Nature Photonics* **7**, 197 (2013).
 - [38] N. Cherroret, T. Karpiuk, B. Grémaud, C. Miniatura, Thermalization of matter waves in speckle potentials, *Phys. Rev. A* **92**, 063614 (2015).
 - [39] S. Nazarenko, A. Soffer, M.-B. Tran, On the wave turbulence theory for the nonlinear Schrödinger equation with random potentials, *Entropy* **21**, 823 (2019).
 - [40] Z. Wang, W. Fu, Y. Zhang, H. Zhao, Wave-turbulence origin of the instability of Anderson localization against many-body interactions, *Phys. Rev. Lett.* **124**, 186401 (2020).
 - [41] T. Scoquart, P.-E. Larré, D. Delande, N. Cherroret, Weakly interacting disordered Bose gases out of equilibrium: From multiple scattering to superfluidity, *Europhysics Letters* **132**, 66001 (2020).
 - [42] N. Cherroret, T. Scoquart, D. Delande, Coherent multiple scattering of out-of-equilibrium interacting Bose gases, *Annals of Physics* **435**, 168543 (2021).
 - [43] D. Psaltis, C. Moser, Imaging with multimode fibers, *Opt. and Photon. News* **27**, 24 (2016).
 - [44] P. Caramazza, O. Moran, R. Murray-Smith, D. Faccio, Transmission of natural scene images through a multimode fibre, *Nat Commun* **10**, 2029 (2019).
 - [45] A. Mecozzi, C. Antonelli, M. Shtaif, Nonlinear propagation in multimode fibers in the strong coupling regime, *Opt. Exp.* **20**, 11673 (2012).
 - [46] A. Mecozzi, C. Antonelli, M. Shtaif, Coupled Manakov equations in multimode fibers with strongly coupled groups of modes, *Opt. Exp.* **20**, 23436 (2012).
 - [47] S. Mumtaz, R.J. Essiambre, G.P. Agrawal, Nonlinear propagation in multimode and multicore fibers: Generalization of the Manakov equations, *J. Lightw. Technol.* **31**, 398 (2013).
 - [48] Y. Xiao, R.-J. Essiambre, M. Desgroseilliers, A.M. Tulino, R. Ryf, S. Mumtaz, G.P. Agrawal, Theory of intermodal four-wave mixing with random linear mode coupling in few-mode fibers, *Opt. Exp.* **22**, 32039 (2014).
 - [49] W. Xiong, P. Ambichl, Y. Bromberg, B. Redding, S. Rotter, H. Cao, Spatiotemporal control of light transmission through a multimode fiber with strong mode coupling, *Phys. Rev. Lett.* **117**, 053901 (2016).
 - [50] J.-P. Fouque, J. Garnier, G. Papanicolaou, and K. Sølna, *Wave Propagation and Time Reversal in Randomly Layered Media* (Springer, 2007).

- [51] See Supplementary Material for the theoretical derivation of the KE (4), for the analytical expressions of the matrices $\mathbf{\Gamma}^D$ and $\mathbf{\Gamma}^{OD}$ used in the simulations, and a complementary description of the experimental methods.
- [52] More exactly, $\mathcal{L}_{\text{kin}}^{\text{eq}} = 1/\lambda_2^{OD}$ where $-\lambda_2^{OD}$ is the second eigenvalue of the matrix $\tilde{\mathbf{\Gamma}}^{OD}$, with $\tilde{\Gamma}_{jl}^{OD} = \Gamma_{jl}^{OD}$ for $j \neq l$ and $\tilde{\Gamma}_{jj}^{OD} = -\sum_{l \neq j} \Gamma_{jl}^{OD}$, the first eigenvalue being $\lambda_1^{OD} = 0$.
- [53] K.-P. Ho, J.M. Kahn, Linear propagation effects in mode-division multiplexing systems, *J. Lightwave Tech.* **32**, 4 (2014).
- [54] R. Weill, B. Fischer, O. Gat, Light-mode condensation in actively-mode-locked lasers, *Phys. Rev. Lett.* **104**, 173901 (2010).
- [55] E. Turitsyna, S. Smirnov, S. Sugavanam, N. Tarasov, X. Shu, S. Babin, E. Podivilov, D. Churkin, G. Falkovich, S. Turitsyn, The laminar-turbulent transition in a fibre laser, *Nature Photon.* **7**, 783 (2013).
- [56] I.S. Gradshteyn and I.M. Ryzhik, *Tables of Integrals, Sums, Series, and Products* (Academic Press, New York, 1980).
- [57] J.R. Fienup, Phase retrieval algorithms: a comparison, *Applied Optics* **21**, 2758 (1982).